Magnetic breakdown and the de Haas–van Alphen effect in $Hg_{1-x}Fe_xSe$

M. M. Miller and R. Reifenberger
Physics Department, Purdue University, West Lafayette, Indiana 47907
(Received 15 December 1986; revised manuscript received 3 December 1987)

Measurements of the de Haas–van Alphen oscillations at $T=0.55$ K as a function of magnetic field direction in single crystal $Hg_{1-x}Fe_xSe$ are reported. Spectral analysis using discrete Fourier transforms reveals the presence of up to six closely spaced frequency components. The angular dependence of the spectral content of the oscillations can be understood with a closed-orbit magnetic breakdown model. Using this model, the first and second harmonics of the de Haas–van Alphen signal for $\mathbf{H}\|[111]$ can be fitted quantitatively. Estimates of the energy difference between the spin-split conduction bands are extracted from this analysis.

I. INTRODUCTION

The ternary diluted magnetic semiconductor (DMS) $Hg_{1-x}Fe_xSe$ has recently been the subject of interest for a number of reasons. It is one of the first examples of an Fe-based DMS and thereby extends the DMS beyond the Mn-based systems which have received much recent attention.[1] Secondly, $Hg_{1-x}Fe_xSe$ was found to exhibit a number of unique properties. Early work showed that the addition of only 0.03 at. % Fe eliminated the electron carrier concentration instability that is well known from prior studies of the binary parent HgSe.[2] Shubnikov–de Haas (SdH) studies have further shown that the presence of Fe greatly *reduces* the low-temperature electronic scattering rate relative to HgSe samples with the same electron concentration. As a result, evidence for spin-dependent transport effect has been reported.[3] More recent studies of the Hall mobility in a number of $Hg_{1-x}Fe_xSe$ samples ($0.0001 \leq x \leq 0.12$) have revealed an anomalous, systematic increase in the mobility as the temperature is lowered.[4–6] Measurements down to 4.2 K in some samples show no evidence for a saturation in the mobility. Taken all together, these results indicate that substantially new physical effects are occurring in this particular ternary system.

These new effects have been attributed to the formation of a 3+ valence state for the substitutional Fe atoms in addition to the Fe^{2+} state that is normally anticipated. The 3+ state is thought to occur naturally in this system because of a coincidence between the *d* levels of Fe with the conduction-band continuum of HgSe. It has also been suggested that the Fe atoms having the 3+ valence state acquire a spatial ordering as the temperature is lowered.[7] If such a spatial ordering occurs, it suggests that a three-dimensional (3D) quasiperiodic "superlattice" naturally forms in this ternary system and is governed by correlation effects similar to the Wigner crystallization phenomena proposed for a free-electron gas. It is crucial to better understand the band structure of $Hg_{1-x}Fe_xSe$ in order to allow a further elaboration of these unusual properties.

For these reasons, a systematic study of the conduction-band structure of $Hg_{1-x}Fe_xSe$ is of considerable importance. Quantum oscillations provide an ideal, **k**-dependent spectroscopy to probe the conduction-band states. Recently, a systematic study of the Shubnikov–de Haas oscillations in $Hg_{1-x}Fe_xSe$ was performed and showed a surprisingly complicated angular dependence.[8] This prior study revealed a strongly anisotropic envelope function, dominated by a long sequence of zeros, that modulated the SdH oscillations. This is an unexpected result since paraboliclike conduction bands should give rise to an isotropic, monotonically increasing envelope function. As will be discussed in this paper, the correct interpretation of these zeros holds the key to a quantitative study of the conduction-band structure in $Hg_{1-x}Fe_xSe$.

The line shape of the SdH oscillations in $Hg_{1-x}Fe_xSe$ should have a common origin with the quantum oscillations in the parent material HgSe. Indeed, zeros in the SdH effect, commonly referred to as "beating effects," have been reported in HgSe over twenty years ago.[9] Roth[10] attributed the beating to the presence of two extremal cross sections of the Fermi surface resulting from inversion asymmetry splitting of the conduction band in the zinc-blende lattice. Roth developed a model using a Hamiltonian that included magnetic breakdownlike coupling of the two Fermi-surface orbits. While this model was able to explain features of the SdH data in HgSe (Ref. 11) and GaSb (Ref. 12) it remains difficult to apply and the results obtained are still somewhat inconclusive.

At this point, it is useful to briefly outline the history behind magnetic breakdown phenomena. Magnetic breakdown effects were first required to interpret unexpected frequency components observed in the de Haas–van Alphen (dHvA) spectra of metals. These unexpected frequency components resulted from electron states tunneling between two different energy bands separated in **k** space by a small energy gap. In metals, where the energy band structure is complicated by Brillouin-zone boundaries, the splitting between two arbitrary bands can become quite small and magnetic breakdown effects are ubiquitous. In semiconductors, however, with paraboliclike conduction bands and low electron concentrations, the relevant energy separation between bands is generally larger. As a result, magnetic break-

down effects have largely been neglected. This situation changes, however, in degenerate semiconductors which lack inversion symmetry. Under these conditions, the twofold band degeneracy is split and small ($\sim$meV) separations between the spin-up and spin-down states are expected. Under these circumstances, magnetic breakdown effects become crucial for the correct interpretation of quantum oscillatory effects.

This point of view was recently emphasized by Reifenberger and Schwarzkopf[13] who developed a closed-orbit magnetic breakdown model for zinc-blende semiconductors with $\mathbf{H}\|[111]$ in order to fit SdH data in HgSe and $Hg_{1-x}Mn_xSe$. This model was simplified in that it did not require detailed knowledge of the band structure but relied, rather, on a knowledge of the geometry of the Fermi-surface orbits. As such, it is ideal for quantifying small changes to the conduction bands and emphasizes the need for more detailed first-principles band-structure calculations to further complement the information extracted from a magnetic breakdown analysis of data.

While the magnetic breakdown model developed in Ref. 13 was able to fit SdH data at high magnetic fields ($H > 1.0$ T), the fact that no more than two zeros were observed casts doubt on the conclusiveness of that study. To conclusively test this model requires the experimental detection of more zeros. As will be demonstrated in this paper and a subsequent one, $Hg_{1-x}Fe_xSe$ is ideal for such a study.

In order to make further progress, careful measurements of the quantum oscillations are required. In general, this requires measurements at low magnetic fields. Lower temperatures are also required in order to improve the signal-to-noise ratio. This paper presents the results of dHvA measurements that were performed on oriented single crystals of $Hg_{1-x}Fe_xSe$ down to temperatures of 0.55 K and for magnetic fields down to 0.2 T. As in SdH measurements, dHvA is useful in investigating the geometry of the Fermi surface but, additionally, dHvA has advantages since the data are less susceptible to ambiguous interpretation. Furthermore, using the field-modulation technique, we have been able to compare the dHvA data quantitatively with a closed-orbit magnetic breakdown model previously described in Ref. 13.

The remainder of this paper is divided into four sections. In Sec. II we review some of the theory relevant to our study of $Hg_{1-x}Fe_xSe$. Sections III and IV describe the experimental apparatus and techniques utilized in this study. Finally, Secs. V and VI present the experimental results and conclusions.

II. THEORY

A. de Haas–van Alphen effect

The dHvA effect is generally described in terms of the well-known Lifshitz-Kosevich formula[14,15]

$$\mathbf{M}_{\rm osc} = -\hat{m}\sum_{r=1}^{\infty}\sqrt{H}\,\frac{I_r K_r B_r \cos(\pi r S)}{\sqrt{r}}\sin\left[2\pi r\frac{F}{H}+\Phi_r\right], \tag{1}$$

$$\hat{m} = \hat{H} - \frac{1}{F}\frac{\partial F}{\partial\theta}\hat{\theta} - \frac{1}{F\sin\theta}\frac{\partial F}{\partial\Phi}\hat{\Phi}\,.$$

The frequency F is directly related to the extremal cross-sectional area of the Fermi surface perpendicular to the applied magnetic field by

$$F = \left[\frac{\hbar}{2\pi e}\right]\mathcal{A}_{\rm ext}\,. \tag{2}$$

Other factors appearing in Eq. (1) are $I_r = X_r/\sinh X_r$ ($X_r = \alpha r T/H$, $\alpha = 2\pi^2 k_B m^*/e\hbar$) and $K_r = e^{-\alpha r T_D/H}$. The Dingle temperature T_D is an effective temperature that provides a measure of impurity and dislocation scattering. The effect of the Landau-level splitting in the applied magnetic field is included by the term $\cos(\pi r S)$ where $S = g_c m^*/2m$. S is a function of the effective mass (m^*) of the electrons and the cyclotron-averaged g factor (g_c). Finally, B_r describes magnetic breakdown effects which may be required by the Fermi-surface geometry.

B. Band structure

The band structure for any narrow-gap zinc-blende semiconductor has been worked out by Kane using $\mathbf{k}\cdot\mathbf{p}$ perturbation.[16] Of particular interest in this study is the lack of inversion symmetry in the zinc-blende lattice. This causes the twofold degeneracy of the conduction band to split since $E(\mathbf{k},\uparrow) \neq E(\mathbf{k},\downarrow)$.[17,18] A schematic band structure ($\mathbf{k}\sim 0$) for HgSe is shown in Fig. 1(a) in which the inversion asymmetry splitting of the Γ_8 bands

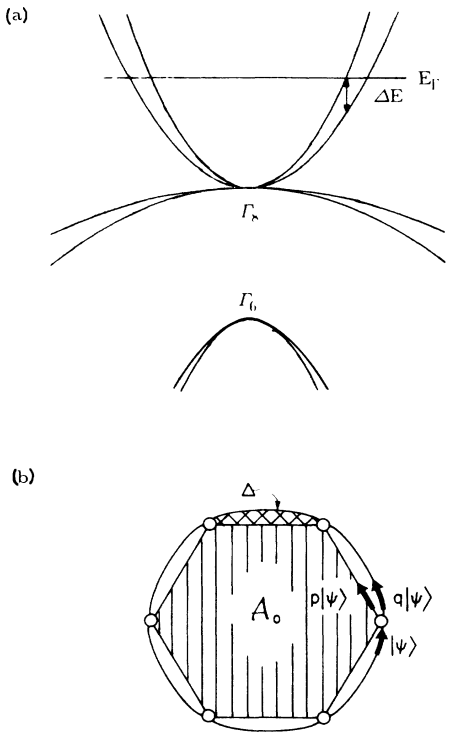

FIG. 1. (a) An illustration of the splitting ΔE in the conduction band due to a lack of inversion symmetry in the crystal lattice. (b) A schematic representation of the resulting Fermi-surface cross section for $\mathbf{H}\|[111]$. The magnetic breakdown junctions are represented by the small circles.

is emphasized. This splitting results in two distinct sheets of the Fermi surface. Seiler *et al.*[19] used Kane's results to show that in the zinc-blende semiconductor HgSe, the form of the Fermi wave vector due to this splitting is given by

$$k_{\rho\pm}^2 \simeq C_0[1-C_1 y_1(\theta,\phi) \mp C_2 y_2(\theta,\phi)] \ . \tag{3}$$

The functions $y_1(\theta,\phi)$ and $y_2(\theta,\phi)$ correspond to warping and to inversion asymmetry, respectively. C_0, C_1, and C_2 exhibit complicated dependence upon the band parameters. Using Eq. (3), the dHvA frequency can be written as a function of the magnetic field direction θ by

$$F_\pm = \frac{\hbar C_0}{2e}\left[1-\frac{C_1}{2\pi}g_1(\theta)\pm\frac{C_2}{2\pi}g_2(\theta)\right] , \tag{4}$$

where $g_1(\theta)$ and $g_2(\theta)$ are the integrated functions of $y_1(\theta,\phi)$ and $y_2(\theta,\phi)$, respectively.

Figure 1(b) shows a schematic model for the Fermi-surface cross section for the [111] orientation ($\theta=55°$) based on Eq. (3). In this model there is an inner and an outer orbit which contribute two frequencies to the dHvA effect that differ by $(\hbar/2\pi e)(6\Delta)=6F_\Delta$. However, at the points marked by the circles it is expected that magnetic breakdown will occur and introduce five additional intermediate frequencies that differ by integer multiples of F_Δ.

C. Magnetic breakdown

For H||[111] it is possible to calculate the magnetic breakdown (MB) function following Ref. 13. However, as will be shown in Sec. IV, it is necessary to include a phase difference between the inner and outer orbits in order to fit the data. (In Ref. 13 this phase difference was implicitly assumed to be zero.) If an additional phase 2δ is assigned to a complete outer orbit (with respect to a phase of zero assigned to a complete inner orbit), then it is straightforward to modify the MB model accordingly. For the orbits shown in Fig. 1(b), it follows that for each difference area Δ added to the inner orbit through MB, an additional phase of $2\delta/6$ must be taken into account. From this reasoning, B_r for $r=1$ and $r=2$ is found to be

$$B_1 = 2(q^6)\cos\left[\frac{6\pi F_\Delta}{H}+\delta\right]+2(6q^4p^2)\cos\left[\frac{4\pi F_\Delta}{H}+\frac{2}{3}\delta\right]+2(6q^4p^2+9q^2p^4)\cos\left[\frac{2\pi F_\Delta}{H}+\frac{1}{3}\delta\right]$$
$$+(6q^4p^2+12q^2p^4+2p^6) , \tag{5a}$$

$$B_2 = 2(q^{12})\cos\left[\frac{12\pi F_\Delta}{H}+2\delta\right]+2(12q^{10}p^2)\cos\left[\frac{10\pi F_\Delta}{H}+\frac{5}{3}\delta\right]$$
$$+2(12q^{10}p^2+54q^8p^4)\cos\left[\frac{8\pi F_\Delta}{H}+\frac{4}{3}\delta\right]+2(12q^{10}p^2+96q^8p^4+112q^6p^6)\cos\left[\frac{6\pi F_\Delta}{H}+\delta\right]$$
$$+2(12q^{10}p^2+126q^8p^4+252q^6p^6+105q^4p^8)\cos\left[\frac{4\pi F_\Delta}{H}+\frac{2}{3}\delta\right]$$
$$+2(12q^{10}p^2+144q^8p^4+360q^6p^6+240q^4p^8+36q^2p^{10})\cos\left[\frac{2\pi F_\Delta}{H}+\frac{1}{3}\delta\right]$$
$$+(12q^{10}p^2+150q^8p^4+400q^6p^6+300q^4p^8+60q^2p^{10}+2p^{12}) . \tag{5b}$$

The probability for MB and reflection are given, respectively, by

$$p=\exp(-H_0/2H) , \tag{6a}$$

$$q=i(1-p^2)^{1/2} , \tag{6b}$$

where the magnetic breakdown field H_0 is given by

$$H_0=\frac{\pi m^*(\Delta E)^2}{e\hbar E_F \sin\phi} . \tag{7}$$

In Eq. (7), ΔE is the energy splitting at the breakdown junction and ϕ is the angle the electron state is turned upon reflection.

In the low-field limit, $H \ll H_0$ ($|\mathbf{p}|\to 0$; $|\mathbf{q}|\to 1$), this model predicts the existence of two frequency components and, as a result, the amplitude of the dHvA oscillations will be periodically reduced to zero by beat modulation effects. The position of the zeros in the amplitude of the oscillations will occur at magnetic fields H_m that are given by the first term of Eq. (5a):

$$(2m-1)\frac{\pi}{2}=6\pi F_\Delta\frac{1}{H_m}+\delta . \tag{8}$$

In this regime, we can write the beat frequency using Eq. (4) as

$$6F_\Delta=\frac{\hbar}{2\pi e}C_0C_2g_2(\theta=55°) . \tag{9}$$

However, as the magnetic field increases, MB effects become more pronounced and the line shape of the oscillations becomes more complicated due to the interference among the additional frequencies appearing in Eq. (5a). In previous SdH studies of HgSe and $Hg_{1-x}Mn_xSe$,[13] data were limited to high magnetic fields ($H > 1$ T) in which no more than two zeros were observed. As a consequence, a convincing verification of the MB model was not possible. $Hg_{1-x}Fe_xSe$, as will be shown, with its high electron concentration ($\sim 5\times 10^{18}$ cm^{-3}) and low Dingle temperatures ($T_D \sim 1.0$ K),[20] is an ideal material to test the predictions of Eq. (5).

D. Origin of the phase difference δ

In order to fit data, a phase difference of 2δ between the inner and outer orbits was required. This phase difference is presumably related to the difference in spin states between the two orbits. To understand this, it is convenient to reconsider the low field limit ($|\mathbf{p}| \to 0$; $|\mathbf{q}| \to 1$) of Eq. (1) and explicitly include the possibility of different spin states for the inner and outer orbits by writing

$$M_{\rm osc} = \sum_{j=1}^{2} \sum_{r=1}^{\infty} A_{j,r} \sin\left[2\pi r\left(\frac{F_j}{H}\right) + \Phi_{j,r} + \pi r S_j\right] . \quad (10)$$

In this case we assume that the inner and outer orbits are described by different spin states given by S_j. For pure spin states, $S_1 + S_2 = 0$ and $S \equiv S_2 - S_1 = gm^*/2m$. The two frequencies, F_1 and F_2, are identified with F_- and F_+ given in Eq. (4). The possibility of spin-dependent scattering[21] can be taken into account by having, in general, that $A_{1,r} \neq A_{2,r}$. Summing over j yields

$$M_{\rm osc} = 2 \sum_{r=1}^{\infty} A_1 \sin\left[2\pi r\frac{F}{H} + \Phi_r\right] \cos\left[6\pi\frac{F_\Delta}{H} + \pi r S\right] , \quad (11)$$

where $F = (F_2 + F_1)/2$ and $F_\Delta = (F_2 - F_1)/6$ as defined earlier. For simplicity, we have assumed that $\Phi_{r,1} = \Phi_{r,2}$ and $A_{r,1} = A_{r,2}$ and have defined $\Phi_r = [\Phi_{1,r} + \Phi_{2,r} + \pi r(S_1 + S_2)]/2$. From these assumptions and the form of Eq. (11), δ in Eq. (5a) can be attributed to the spin splitting between the two bands and is given by

$$\delta = \pi S = \pi\frac{g^* m^*}{2m} , \quad (12)$$

where g^* is an "effective" cyclotron-averaged g factor. Strictly speaking, it is not possible to assign a pure spin state to each band, particularly in the presence of a magnetic field. However, the approach outlined above has the possibility of including the exchange interaction of electrons with magnetic ions into a simple band-structure model.

III. EXPERIMENTAL CONSIDERATIONS

To observe the dHvA effect, we employed the field modulation technique[22] in which a small ac modulation field, $h_0\cos(\omega t)$ ($\omega/2\pi \sim 40$–100 Hz), is superimposed on the larger quasistatic field, H, where $h_0/H \ll 1$. A voltage induced in a noninductive balanced coil surrounding the sample is measured using phase-sensitive detection with a lock-in amplifier. It is well known that the use of this technique introduces an additional magnetic-field-dependent Bessel function factor in Eq. (1). In order to analyze our data, the dHvA signal for one frequency F takes the form

$$V_{\rm osc} = \sum_{n=1}^{\infty} \sum_{r=1}^{\infty} A_r B_r J_n(\beta_r) \sin\left[2\pi r\frac{F}{H} + \Phi_r\right] \sin(n\omega t) \quad (13)$$

where

$$\beta_r = \frac{2\pi r F h_0}{H^2} .$$

The magnetic field was generated using an iron core magnet capable of rotating in the horizontal plane and of generating homogeneous fields up to 1.5 T. A nuclear magnetic resonance (NMR) calibrated gaussmeter was used to measure the magnetic field and the data were digitized in equal field increments and stored on computer for later analysis with the discrete Fourier transform (DFT). Temperatures as low as 0.5 K were achieved by use of a ^{3}He evaporation cryostat.

The pickup coil is a composite of two concentric coils having equal turn areas so as to be inductionless when no sample is in place. The inner coil (primary) consists of approximately 2200 turns of 0.04-mm-diam wire while the outer coil (secondary) has approximately 700 turns of 0.07-mm-diam wire. The output from this pickup coil was connected to a small, Pb-shielded transformer (gain ~ 50) that was integrally built into the lower half of the ^{3}He probe. The output of the transformer was then directed to a phase-sensitive detector.

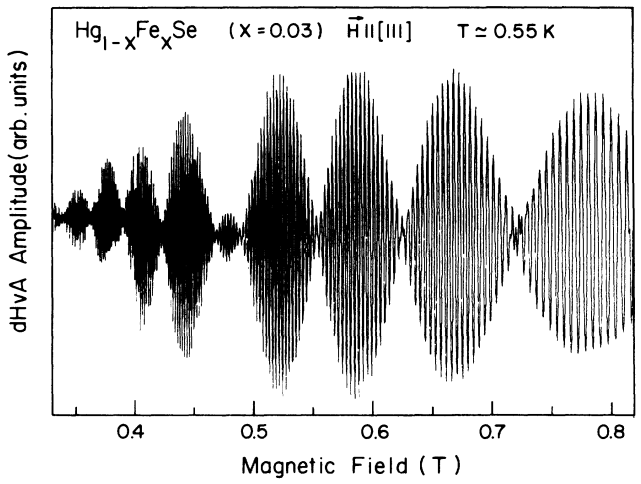

FIG. 2. dHvA oscillations for H||[111] in $Hg_{1-x}Fe_xSe$ ($x = 0.03$) at $T \simeq 0.55$ K. The Bessel function, $J_2(\beta)$, has not been removed from the data. The modulation field used was $h_0 = 7.4$ G.

The crystals used in this study were grown by the Bridgman technique. The as-grown ingots were first oriented by standard x-ray backreflection techniques to an accuracy of $\pm 1°$. The ingots were then cut into parallelepipeds of dimensions of $\sim 1.0 \times 1.0 \times 5.0$ mm^3 using a precision wire saw. A freshly cut sample is cleaned in a 10% bromine-methanol etch solution for less than a minute. Microprobe analysis was done to check the Fe content for those samples with $x > 0.01$.[2]

The techniques utilized in this study as well as the anomalously low scattering rates in $Hg_{1-x}Fe_xSe$ allowed us to observe dHvA oscillations at quite low magnetic fields. Figure 2 shows dHvA oscillations for $\mathbf{H} \| [111]$ and represents the typical quality of the data taken for this study. The modulation envelope of the dHvA oscillations due to beating effects discussed above is clearly evident from this data.

IV. METHOD OF DATA ANALYSIS

The beating effects in $Hg_{1-x}Fe_xSe$ suggest the presence of two or more frequencies differing by only a few percent. Earlier SdH investigations have shown these line shapes are not simply due to two-frequency beating.[8] To extract the constituent frequencies without resorting to oversimplified models, we use the DFT. Prior to DFT the data were first multiplied by a Gaussian window function to ensure that the DFT peaks would be Gaussians with a known full width at half maximum, $\Gamma = 1.0$ T. Since the data evidently contain more than one frequency component, the DFT comprised of m frequency components was fitted by least-squares techniques to a sum of m Gaussians plus a linear background given by[23]

$$G(f) = \sum_{j=1}^{m} b_j e^{-4\ln 2(f-f_j)^2/\Gamma^2} + cf + d \ . \tag{14}$$

This approach was followed to provide impartial estimates for the frequency components. In fitting the DFT spectrum, the number of frequencies (m), the frequency values (f_j), and the DFT amplitudes (b_j) as well as c and d are given as initial estimates. Least-squares fitting is done on a computer with m and Γ fixed while f_j, b_j, c, and d are varied. The difference between the fitted spectrum and the actual spectrum is plotted and used to determine the appropriateness of the fit. However, this technique has limitations due to the interference of the overlapping frequency components. This interference can cause frequencies to be shifted and even suppress weaker frequency components. This situation was considered by Kamm[24] and in more detail by Miller.[25] Based on the relevant parameters for this experiment, the minimum separation between two dHvA frequency components to allow unambiguous resolution is ~ 1.0 T.

V. EXPERIMENTAL RESULTS AND DISCUSSION

A. Angular dependence of spectral content

The results of an angular survey of dHvA data from $Hg_{1-x}Fe_xSe$ ($x \simeq 0.03$) is presented in this section. The data were taken for $\mathbf{H}$ rotating in the (001) and (110) planes. As in earlier SdH data,[8] the dHvA oscillations show a large number of zeros in the amplitude over a wide range of angles. Figure 3 compares the angular dependence of the zero positions in both rotation planes for SdH and dHvA measurements. It should be noted that the SdH measurements were taken at $T = 1.3$ K while the dHvA measurements were taken at $T = 0.55$ K. However, there is virtually no difference in the structure or position of the zeros. From dHvA measurements, we have found that the zero positions change by less than 1% between these two temperatures. Because of the inherent sensitivity of dHvA signals to the entire sample, it can be concluded that the beating effects in this material are not an artifact of SdH measurements and result from bulk phenomena in these materials. In particular, it should be noted that the zeros cannot be due to sample inhomogeneities. The angular dependence is reproducible from sample to sample; the sample used in the SdH studies was not the same sample used in this study. Furthermore, microprobe analysis has shown the boules from which the samples were obtained are characterized by a uniform distribution of the constituents. However, a presentation of zero positions by itself does not allow a quantitative understanding of the band structure which produces these features.

Using the above spectral analysis techniques, we can go beyond measurement of the zero positions. Figure 4 shows the resulting DFT and least-squares fit of typical data shown in Fig. 2. The residual, shown in the bottom part of Fig. 4, indicates that an acceptable fit was obtained. Based on our analysis, we conclude that there are two dominant frequency components and at least four

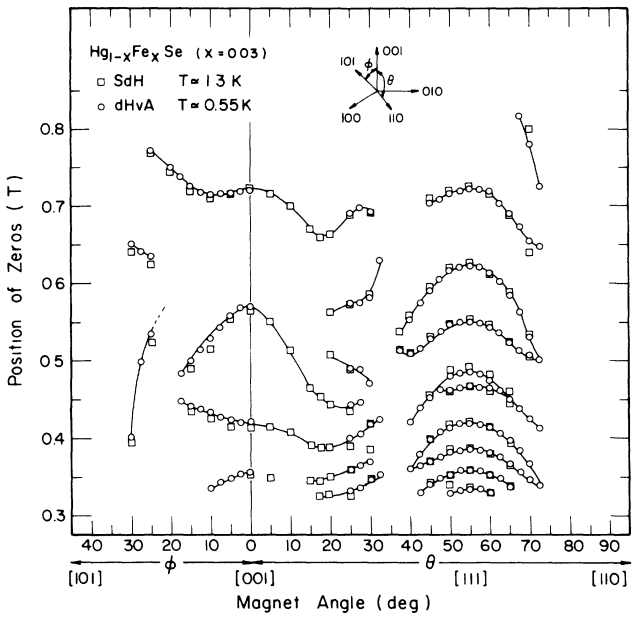

FIG. 3. The position of zeros in $Hg_{1-x}Fe_xSe$ ($x = 0.03$) as a function of magnet angle for two different planes of rotation. The squares correspond to zeros in the SdH oscillations for $T \simeq 1.3$ K while the circles correspond to zeros in the dHvA oscillations for $T \simeq 0.5$ K.

weak frequency components in this data. In view of the problem of suppression of frequencies due to interference,[25] it is possible that other frequency components are present. Using this DFT technique the spectral analysis of dHvA data in the two rotation planes was obtained (Fig. 5). Because the signal disappears when **H** is perpendicular to the coil axis, data are restricted to a limited range. In plotting these data, an arbitrary criterion was set such that dominant frequency components would be indicated with solid dots while those with a Fourier-transform peak less than half the largest peak would be indicated with open circles. While the structure is quite complicated, some important features can be pointed out.

First, for **H**||[110] the DFT yields only one frequency which is expected since there is no evidence of beating in the oscillations for this orientation.[3,8] Second, the number of frequency branches increases dramatically when one leaves the [110] orientation; as many as six branches appear, though not all frequencies are dominant. However, in the (110) rotation plane there are five clearly separated, *dominant* frequencies for θ near 30°. The presence of so many frequencies is difficult to explain in terms of a simple Fermi surface. Neglecting inversion asymmetry, the Fermi surface is expected to be only slightly warped and should contribute a single, weakly angle-dependent dHvA frequency. Even if one includes inversion asymmetry so that there are two sheets of the Fermi surface present, there should only be a maximum of two frequency components present. The additional frequencies can only be explained if MB effects occur between the two spin-split Fermi surfaces.

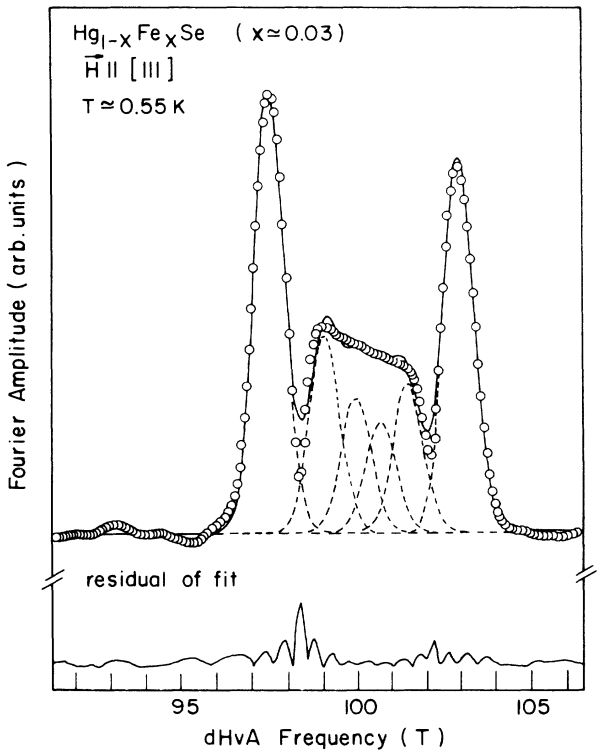

FIG. 4. The discrete Fourier transform (DFT) (circles) performed on the dHvA oscillations in $Hg_{1-x}Fe_xSe$ ($x=0.03$) for **H**||[111] shown in Fig. 2. The windowing Gaussian was chosen so that $\Gamma=1.0$ T. The dashed lines are the individual Gaussians fitted to the DFT and the solid line is the sum of the fitted Gaussians. The curve below (residual) is the difference between the fit and the DFT.

The entire dHvA frequency spectrum should be accounted for by generating the frequencies predicted by the MB model. The predictions of this model, shown by the solid lines in Fig. 5, rely on the reasonable assumption that magnetic breakdown will occur whenever the two spin-split orbits make their closest approach to one another. From the form for the Fermi wave vector in Eq. (3) and taking into account all possible magnetic breakdown orbits, a theoretical frequency spectrum can be numerically generated. C_0, C_1, and C_2 were adjusted until an acceptable fit was made with the spectral data. The values of these parameters are

$$C_0=2.9\times10^{17}\ \mathrm{m}^{-2}\ ,$$

$$C_1=-0.20\ ,$$

$$C_2=0.072\ .$$

C_1 is the coefficient related to warping of the Fermi surface and the negative value is consistent with the results of Galazka *et al.*[26] in HgSe.

While this model does not reproduce every measured frequency branch, there are two encouraging features. First, the overall angular dependence of the frequency branches can be made to agree quite well. Furthermore, in the vicinity of the [111] orientation, the data and the theory agree quite well for the high- and low-frequency branches. The intermediate frequencies do not matchup so well but, in view of the possible suppression of frequency components due to the interference effects mentioned earlier,[25] this does not seem surprising. Second, the model that we used to generate the theoretical frequency branches does *not* take into account the probability of having that particular frequency present. For example, for **H**||[110], the model predicts nine frequencies while only one is measured. The single frequency is almost certainly the result of complete magnetic breakdown. A more quantitative analysis of data based on magnetic breakdown considerations will now be discussed.

B. Magnetic breakdown analysis, H||[111]

1. Low-field zero positions

Due to the large number of beat zeros observed in the sample with $x=0.001$, we shall concentrate on these data for comparison to the model. Figure 6 is a plot of $(2m-1)\pi$ versus $1/H_m$, where H_m is the beat zero position defined in Eq. (8). The choices for m were arbitrarily made so that the intercept of the fitted line would be as close to zero as possible. A least-squares straight-line fit was performed for the solid data points. The slope of the fitted line yields $F_\Delta=0.97$ T while the intercept yields $\delta=\pi/2$. This nonzero intercept provides a compelling

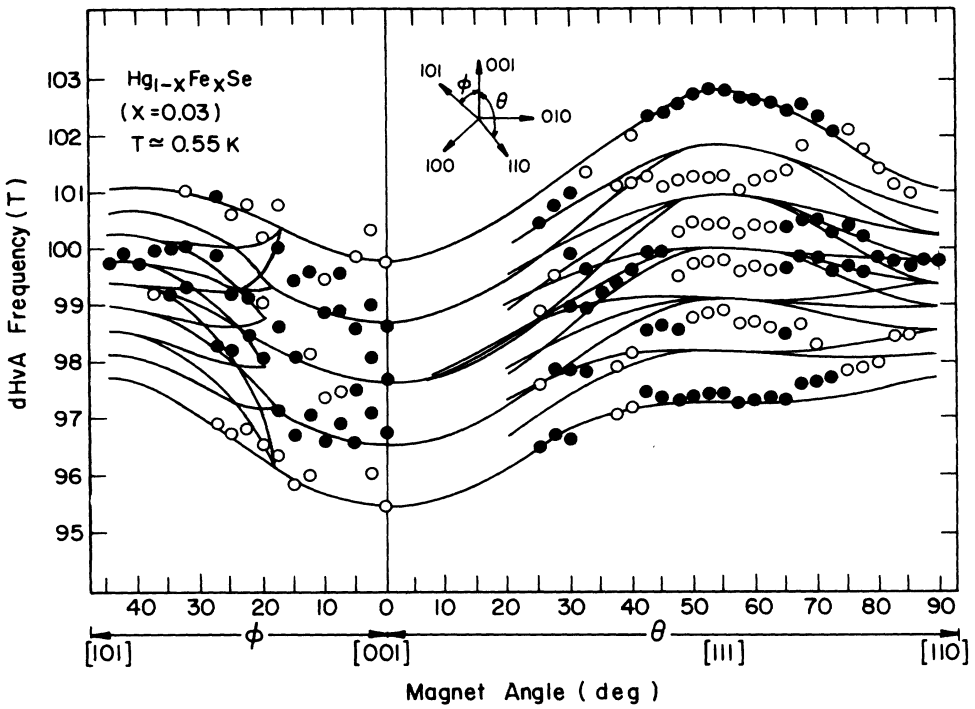

FIG. 5. The discrete Fourier transform spectrum as a function of magnet angle for $Hg_{1-x}Fe_xSe$ ($x=0.03$). The frequency components were extracted using least-squares fitting as in Fig. 4. The solid dots represent dominant frequency components while the open circles represent weak frequency components. The solid lines are the theoretical frequency branches generated using a magnetic breakdown model.

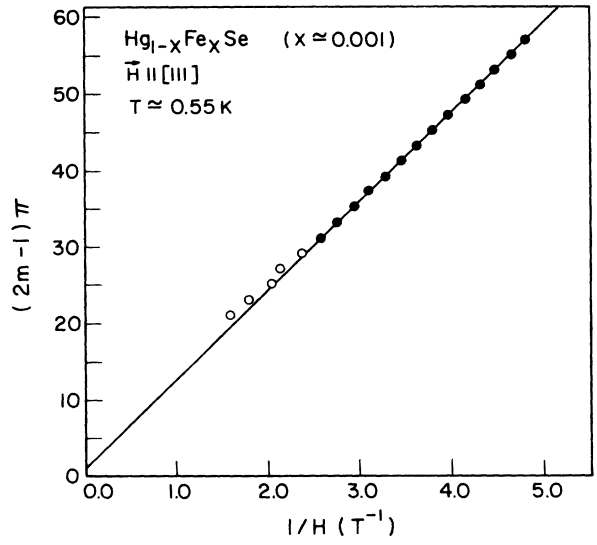

FIG. 6. This plot illustrates the simple beating for H||[111] at low magnetic fields. The zeros (solid dots) are indexed as $(2m-1)\pi$ and plotted vs their position, $1/H_m$. For $H \lesssim 0.4$ T ($1/H \gtrsim 2.5$ T^{-1}) simple beating is evidenced by the straight line. The slope of this line gives F_Δ while the intercept yields δ. For $H > 0.4$ T magnetic breakdown effects are seen in the deviation of the zeros from the straight line. These zeros are indicated by open circles.

experimental motivation for including δ in Eqs. (5a) and (5b). The values of F_Δ and δ are also consistent with those determined by more detailed Fourier analysis. Data points beyond $H \simeq 0.4$ T, indicated by the open circles, were not included in this fit because MB effects begin to become important for higher magnetic fields as is evidenced by the deviation from the straight-line fit of the zero positions in this figure. The same analysis was done for $x=0.03$, giving $F_\Delta = 0.89$ T and $\delta = \pi$.

2. *Magnetic breakdown effects*

For $H \gtrsim 0.4$ T, MB effects become important and a well-reproduced feature appears in the beating pattern for H||[111] that is a signature of MB. A small beat envelope appears for $H \sim 0.5$ T for $x=0.001$ as shown in Fig. 7(a). This feature can also be seen in the $x=0.03$ sample for $H \sim 0.48$ T (see Fig. 2) and arises due to the presence of the additional frequencies that occur as magnetic breakdown effects become important. Using Eq. (5a) it is possible to understand how this anomaly arises. Figures 8(a)–8(d) show the four individual terms in Eq. (5a) as a function of magnetic field. Figure 8(e) shows the sum of these four terms. Since this sum will modulate the experimental data, we plot in Fig. 8(e) the beat envelope [equivalent to plotting both B_1 and $-B_1$ in Eq. (5a)] in order to more clearly demonstrate the line shape resulting from the multiplicative breakdown factor. The beating anomaly observed in the data [Figs. 2 and 7(a)] is

reproduced in the model calculation [Fig. 8(e)]. The position of the beating anomaly [indicated in Fig. 8(e) by the arrows] results when the second and third terms of Eq. (5a) destructively interfere with the first term and cause a reduction in the MB envelope function. It is interesting to note that for the parameters used in Fig. 8, the beat anomalies repeat every sixth beat. This is due to the sixfold symmetry of the model and shall be discussed later in this paper.

Measurement of the second-harmonic content ($r=2$) permits a comparison of the data to the predictions of Eq. (5b). In order to stringently test the MB model, we used the modulation field technique in order to enhance the second-harmonic contribution of the dHvA oscillations relative to that of the fundamental. The low Dingle temperature of the $x=0.001$ sample further provides us with the opportunity to accurately measure the second-harmonic content of the dHvA oscillations. Figure 7(a) shows the results of these measurements. In the upper part of this figure is the dHvA data (mainly comprised of the fundamental dHvA harmonic) that were measured by detecting on the second harmonic of the modulation field frequency ($n=2$) with $h_0 \simeq 9.0$ G. Directly below this is the mainly second dHvA harmonic data which was detected on the tenth harmonic ($n=10$) of the modulation field frequency. The amplitude of the modulation field was set to $h_0 \simeq 22.0$ G in order to suppress the fundamental dHvA oscillation. In this case, the ratio of the amplitude of the second harmonic to the fundamental has been enhanced through the Bessel function term by a factor of about 100 relative to the $n=2$ case.

The second-harmonic dHvA data shows an interesting feature at the same magnetic field that the fundamental harmonic dHvA beat anomaly is observed. In particular, a shallow minimum for $H \simeq 0.5$ T is observed. This anomaly can be explained in terms of magnetic breakdown effects. Figures 7(b)–7(d) show theoretical fits using Eqs. (5a), (5b), and (13). Figure 7 demonstrates very clearly that these measurements provide a great deal of sensitivity to the determination of the magnetic break-

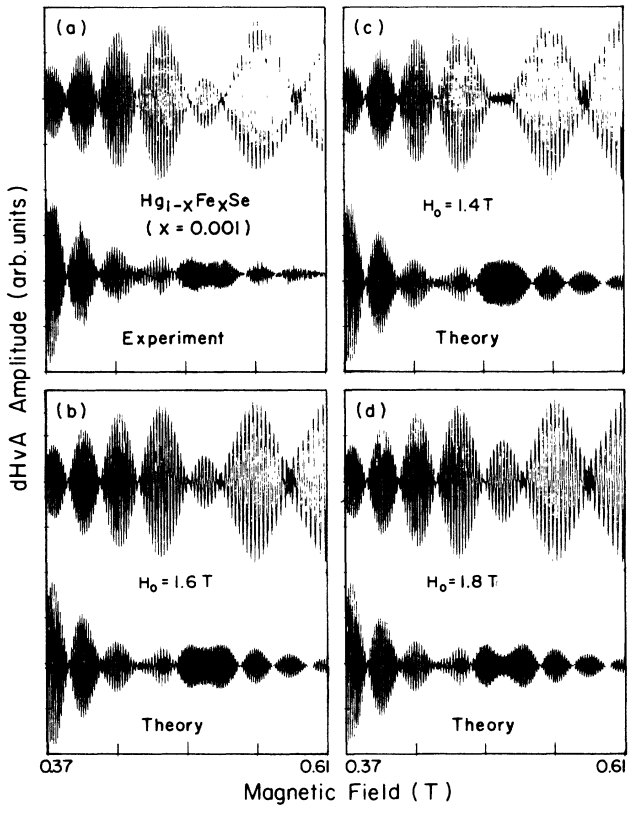

FIG. 7. (a) Experimental dHvA data taken at $T \simeq 0.55$ K for $\mathbf{H} \| [111]$ in $Hg_{1-x}Fe_xSe$ with $x \sim 0.001$. The upper trace was taken on the second harmonic of the modulation field frequency ($n=2$) with $h_0 \simeq 9$ G while the lower trace was obtained by detecting on $n=10$ with $h_0 \simeq 22$ G. (b), (c), and (d) show the theoretical fits to the experimental data treating the magnetic breakdown field H_0 as an adjustable parameter. All essential features in the amplitude of the oscillations are correctly predicted by the magnetic breakdown model with $H_0 \simeq 1.6$ T.

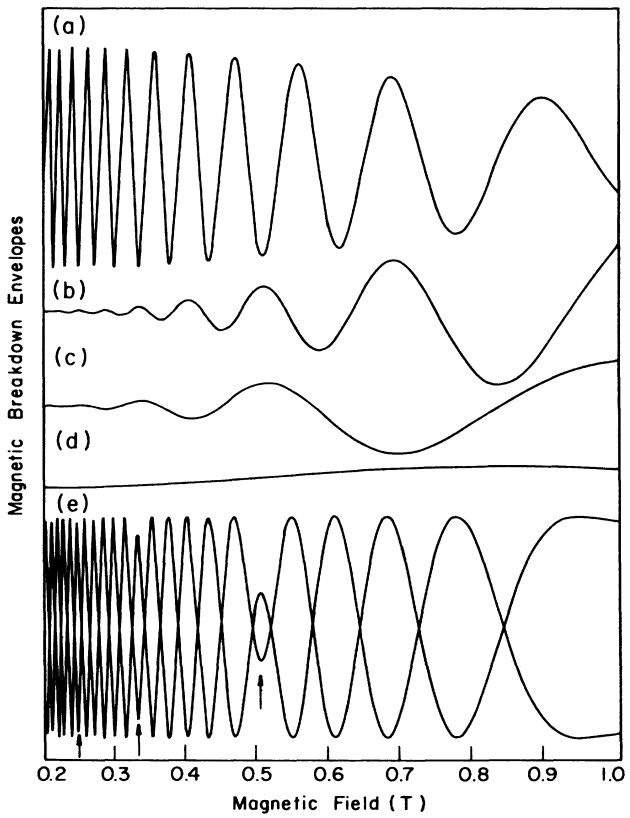

FIG. 8. This plot shows the individual terms of Eq. (5a) as a function of magnetic field with $H_0=1.6$ T, $F_\Delta=0.97$ T, and $\delta=\pi/2$. The individual terms are given as (a) $2(q^6)\cos[6\pi F_\Delta/H)+\delta]$, (b) $2(6q^4p^2)\cos[(4\pi F_\Delta/H)+\frac{2}{3}\delta]$, (c) $2(6q^4p^2+9q^2p^4)\cos[(2\pi F_\Delta/H)+\frac{1}{3}\delta]$, and (d) $(6q^4p^2+12q^2p^4+2p^6)$. The sum of these four terms gives the magnetic breakdown function B_1 and is shown in (e). The anomalous beats, which result from destructive interference between (a), (b), and (c), are indicated by the arrows.

down field H_0. In this case, it was found that $H_0 = 1.6$ T provided the best fit to the data. Using Eq. (7) and assuming a parabolic band with mass $m^* = 0.066 m_0$,[27] we find $\Delta E = 11.6 \sin^{1/2}\phi$ meV. The factor $\sin^{1/2}\phi$ is difficult to calculate precisely because it requires a detailed knowledge of the energy bands. However, it is easy to estimate that ϕ will be between 60° and 160°, giving a value of ΔE between 10.8 and 6.8 meV. An independent estimate for ΔE can be obtained from the beat frequency $6F_\Delta$. For a parabolic band we can write

$$\langle \Delta E \rangle_{\text{orb}} = \frac{\hbar e}{m^*}(6F_\Delta) , \tag{15}$$

which gives $\langle \Delta E \rangle_{\text{orb}} = 10.2$ meV. In this case $\langle \Delta E \rangle_{\text{orb}}$ is the *orbitally averaged* inversion asymmetry energy splitting and should be larger than ΔE determined from the magnetic breakdown field. The reasonable agreement between these two values provides further evidence for the reliability of our analysis.

3. *Threefold symmetry*

Up to now we have considered the H||[111] orientation to have sixfold symmetry in accordance with the Kane model.[16] However, a feature of our data that cannot be explained in terms of this sixfold symmetry provides strong evidence for a threefold symmetry at this orientation. Figure 9 shows the dHvA oscillations over an extended range of magnetic field between $H = 0.35$ and 0.8 T. The arrows point to the familiar anomalous beats that were earlier explained in terms of MB. It is interesting to note that these anomalous beats occur every *third* beat. The sixfold model predicts this anomaly at every *sixth* beat [see Fig. 8(e)]. The six beat period occurs essentially from the interference between the first, second, and third terms of Eq. (5a).

In order to reproduce the one-in-three anomalous beat pattern, it is necessary to reduce the sixfold symmetry inherent in our model to one having only threefold symmetry. Figures 10(a) and 10(b) show two possible threefold symmetry models for the H||[111] orientation. In Fig. 10(a) we have essentially the same model as Fig. 1(b) except that there are two magnetic breakdown fields, $H_{0,1}$ and $H_{0,2}$. If $H_{0,2}$ is significantly larger than $H_{0,1}$ then at low magnetic fields, the magnitude of the third term in Eq. (5a) is enhanced relative to the second term, thereby reproducing the three-beat periodicity of the beat anomaly.

The actual magnetic breakdown function can be calculated in much the same way as that of the sixfold model. However, since this model would involve an additional fitting parameter we shall not attempt to draw quantitative conclusions from it. Another way of breaking the sixfold symmetry is to allow the difference areas to become inequivalent. This possibility is sketched in Fig. 10(b). B_r for this situation has not been calculated. Again, it would require an additional fitting parameter to model the two distinct difference areas.

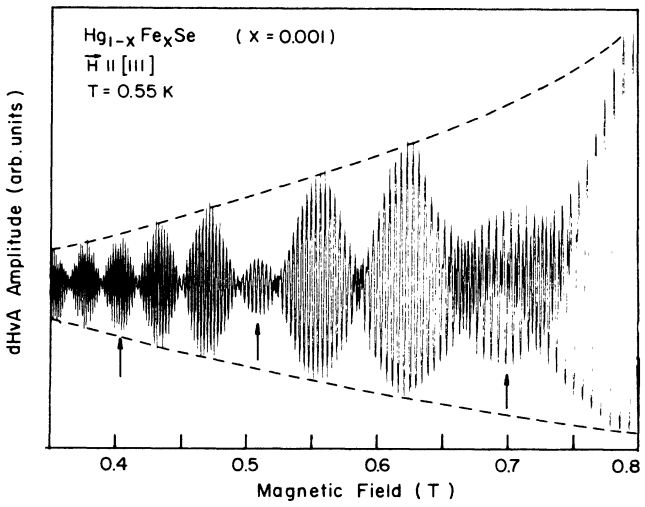

FIG. 9. dHvA oscillations for H||[111] over an extended field range for $x = 0.001$ and $T = 0.55$ K. The anomalous beats are seen every third beat rather than every sixth beat. This suggest that a threefold symmetric model for the Fermi surface may be more appropriate.

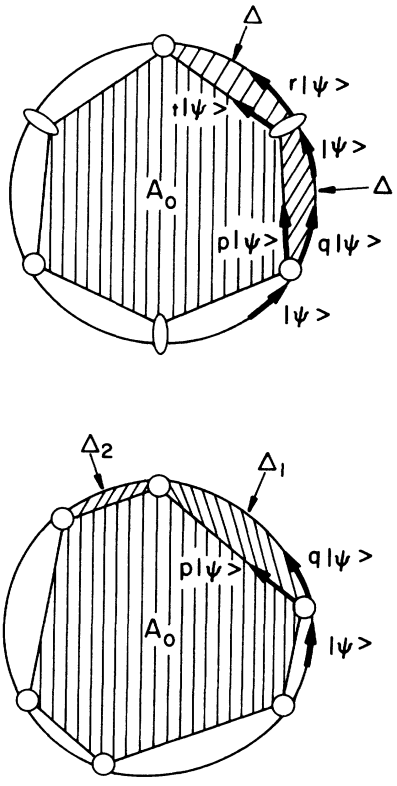

FIG. 10. Two possible threefold symmetric orbit models for H||[111]. (a) This orbit has two different magnetic fields, $H_{0,1}$ and $H_{0,2}$, with breakdown and reflection probabilities, p and q, and t and r, respectively. There are six equal difference areas, Δ. (b) This orbit has six equal magnetic breakdown fields but with two different difference areas, Δ_1 and Δ_2.

VI. SUMMARY AND CONCLUSIONS

In this paper, we have presented the results of the first dHvA study in $Hg_{1-x}Fe_xSe$. We have shown that a closed-orbit MB model proposed in Ref. 13 is crucial to understanding the dHvA oscillations in this material. Specifically, we have shown that for $\mathbf{H}\|[111]$, the dHvA data are in qualitative and quantitative agreement with this model. For sufficiently low magnetic fields such that MB is negligible, the quantum oscillations are unambiguously characterized by simple beating between two slightly different orbits that result from the inversion asymmetry splitting of the conduction band. At higher magnetic fields when MB becomes important, a line-shape anomaly occurs that is quantitatively accounted for by this MB model. This MB analysis has allowed a determination of the inversion asymmetry splitting (8.8 ± 2.0 meV). This is consistent with the orbitally averaged inversion asymmetry splitting (10.2 meV) determined from the low-field beat frequency. Our ability to extract these values emphasizes the need for more precise first-principles band-structure calculations in this material. While it is not possible to obtain such detailed agreement between data and the band structure for orientations different than $\mathbf{H}\|[111]$, we were still able to show that the angular dependence of the spectral content is in qualitative agreement with the Kane model.

In conclusion, we have presented a MB analysis of the dHvA oscillations in $Hg_{1-x}Fe_xSe$. While we have concentrated on $Hg_{1-x}Fe_xSe$ with $x=0.001$ and $\mathbf{H}\|[111]$, the framework developed in this paper should apply generally to all narrow-gap semiconductors which lack inversion symmetry. In a future paper we shall present a systematic study of $Hg_{1-x}Fe_xSe$ as a function of Fe content utilizing the analysis techniques described above.

ACKNOWLEDGMENTS

This work was supported by the National Science Foundation (NSF) through Grant No. DMR 86-10368. The aid of P. H. Keesom in the design and construction of the ^{3}He evaporation cryostat is gratefully acknowledged. We wish to thank M. Vaziri for his assistance and interest in this work. We also wish to thank J. Kossut and G. Crabtree for helpful comments during the initial stages of this study. The expertise of U. Debska in the growth of the crystals used in this study is also greatly appreciated. One of us (M.M.) acknowledges support from the Eastman Kodak Company.

[1] J. K. Furdyna, J. Vac. Sci. Technol. **A4**, 2002 (1986).
[2] M. Vaziri, U. Debska, and R. Reifenberger, Appl. Phys. Lett. **47**, 407 (1985).
[3] M. Vaziri and R. Reifenberger, Phys. Rev. B **32**, 3291 (1985).
[4] F. Pool, J. Kossut, U. Debska, and R. Reifenberger, Phys. Rev. B **15**, 3900 (1987).
[5] A. Mycielski, P. Dzwonkowski, B. Kowalski, B. Orlowski, M. Dobrowolska, M. Arciszewska, W. Dobrowolski, and J. M. Baranowski, J. Phys. C **19**, 3605 (1986).
[6] N. G. Gluzman, N. D. Sabirzyanova, I. M. Tsidilkovskii, L. D. Paranchich, and S. Y. Paranchich Fiz. Tekh. Poluprovodn. **20**, 94 (1986) [Sov. Phys.—Semicond. **20**, 55 (1986)].
[7] J. Mycielski, Solid State Commun. **60**, 165 (1986).
[8] M. Vaziri and R. Reifenberger, Phys. Rev. B **33**, 5585 (1986).
[9] C. R. Whitsett, Phys. Rev. **138**, A829 (1965).
[10] L. M. Roth, Phys. Rev. **173**, 755 (1968).
[11] L. M. Roth, S. H. Groves, and P. W. Wyatt, Phys. Rev. Lett. **19**, 576 (1967).
[12] D. G. Seiler and W. M. Becker, Phys. Rev. **183**, 784 (1969).
[13] R. Reifenberger and D. A. Schwarzkopf, Phys. Rev. Lett. **50**, 907 (1983).
[14] I. M. Lifshitz and A. M. Kosevich, Zh. Eksp. Teor. Fiz. **29**, 730 (1955) [Sov. Phys.—JETP **2**, 636 (1956)].
[15] D. Shoenberg, in *Magnetic Oscillations in Metals* (Cambridge University Press, Cambridge, England, 1984).
[16] E. O. Kane, in *Semiconductors and Semimetals,* edited by R. K. Willardson and A. C. Beer (Academic, New York, 1966), Vol. 1, p. 75.
[17] R. H. Parmenter, Phys. Rev. **100**, 573 (1955).
[18] G. Dresselhaus, Phys. Rev. **100**, 580 (1955).
[19] D. G. Seiler, R. R. Galazka, and W. M. Becker, Phys. Rev. B **3**, 4274 (1971).
[20] M. M. Miller and R. Reifenberger, Phys. Rev. B (to be published).
[21] R. J. Higgins and D. H. Lowndes, in *Electrons at the Fermi Surface,* edited by M. Springford (Cambridge University Press, Cambridge, England, 1980), p. 393.
[22] R. W. Stark and L. R. Windmiller, Cryogenics **8**, 272 (1968).
[23] R. D. B. Fraser and E. Suzuki, in *Spectral Analysis: Methods and Techniques,* edited by James A. Blackburn (Dekker, New York, 1970), p. 199.
[24] G. N. Kamm, J. Appl. Phys. **49**, 5951 (1978).
[25] M. M. Miller, Ph.D thesis, Purdue University, 1987.
[26] R. R. Galazka, W. M. Becker, and D. G. Seiler, in *The Physics of Semimetals and Narrow-Gap Semiconductors,* edited by D. L. Carter and R. T. Bate (Pergamon, New York, 1971), p. 481.
[27] This mass is that for HgSe with the same electron concentration and was also experimentally determined. See Ref. 20.

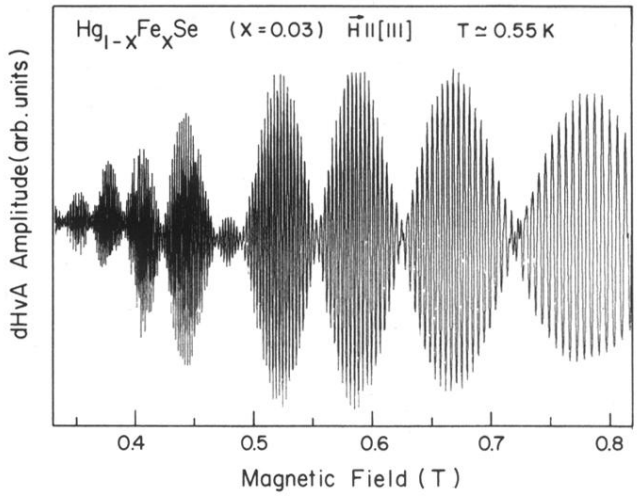

FIG. 2. dHvA oscillations for $\mathbf{H}\|[111]$ in $Hg_{1-x}Fe_xSe$ ($x=0.03$) at $T\simeq 0.55$ K. The Bessel function, $J_2(\beta)$, has not been removed from the data. The modulation field used was $h_0=7.4$ G.

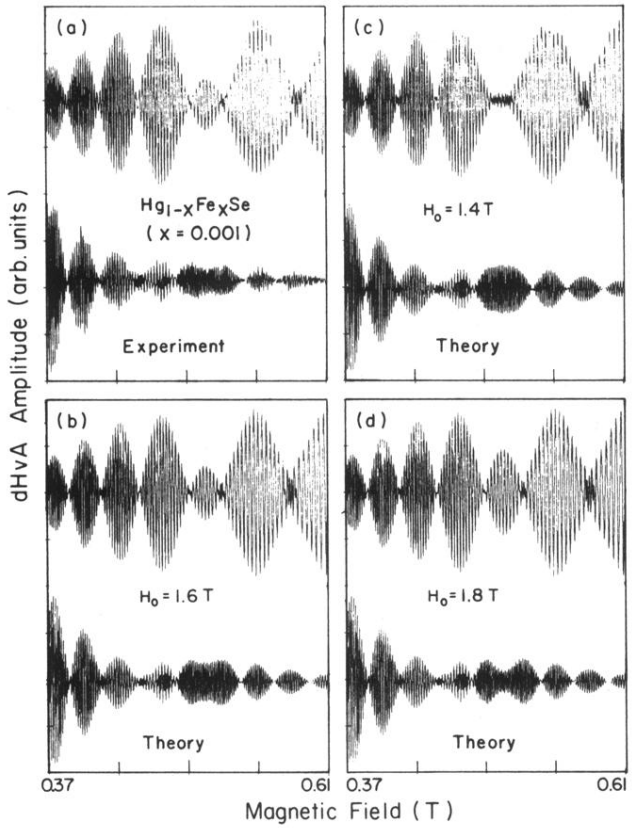

FIG. 7. (a) Experimental dHvA data taken at $T \simeq 0.55$ K for $\mathbf{H} \| [111]$ in $Hg_{1-x}Fe_xSe$ with $x \sim 0.001$. The upper trace was taken on the second harmonic of the modulation field frequency ($n=2$) with $h_0 \simeq 9$ G while the lower trace was obtained by detecting on $n=10$ with $h_0 \simeq 22$ G. (b), (c), and (d) show the theoretical fits to the experimental data treating the magnetic breakdown field H_0 as an adjustable parameter. All essential features in the amplitude of the oscillations are correctly predicted by the magnetic breakdown model with $H_0 \simeq 1.6$ T.

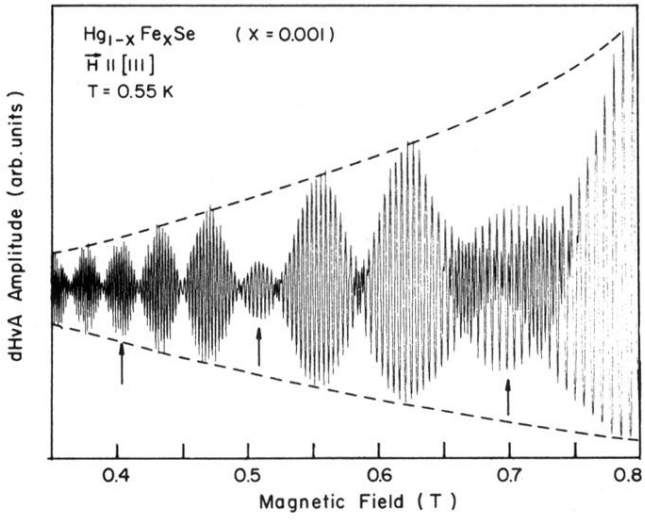

FIG. 9. dHvA oscillations for $\mathbf{H}\|[111]$ over an extended field range for $x=0.001$ and $T=0.55$ K. The anomalous beats are seen every third beat rather than every sixth beat. This suggest that a threefold symmetric model for the Fermi surface may be more appropriate.